Intramolecular energy-transfer processes induced by an external electric field

Vladimir I. Makarov,[1,2] Sergei A. Kochubei,[3] and Igor V. Khmelinskii[4]
[1]*Department of Chemistry, University of Puerto Rico, Rio Piedras, P.O. Box 23346, San Juan 00931-3346, Puerto Rico*
[2]*Institute of Chemical Kinetics and Combustion, RAS, Instituskaya 3, Novosibirsk 630090, Russia*
[3]*Institute of Semiconductor Physics, SB RAS, Novosibirsk 630090, Russia*
[4]*Universidade do Algarve, FCT, P8000-117 Faro, Portugal*
(Received 16 January 2003; revised manuscript received 21 May 2003; published 8 October 2003)

The influence of an external electric field on the state dynamics of electronically excited molecules was analyzed. The electric field was shown to affect the $\Delta S=0$ internal conversion transitions. It was found that in the presence of an external electric field, the lifetime of the acetylene fluorescence decreases, while the emission amplitude remains constant. The theory developed was applied to acetylene excited into single rotational levels of the $(\tilde{A}^1A_u)V^2K^{l=0,1,2}$ vibronic states, which are below the ground-state dissociative threshold. It was proposed that levels of the $(\tilde{A}^1A_u)V^2K^{l=0,1,2}$ vibronic states are coupled by a field to ''quasiresonance'' levels of the $\tilde{X}\,^1\Sigma_g^+$ electronic ground state. Dynamics of the system evolution over the vibrational energy spectrum of the $\tilde{X}\,^1\Sigma_g^+$ electronic ground state was investigated using its IR emission kinetics.

DOI: 10.1103/PhysRevA.68.043403 PACS number(s): 32.60.+i

I. INTRODUCTION

The purpose of physical kinetics is to study intramolecular as well as intermolecular energy evolution phenomena. Usage of narrow-band pulsed laser radiation creates a unique capacity to prepare well-defined initial states of the quantum system studied, and to monitor their subsequent time evolution. Time evolution of an initially prepared state is governed by various relaxation channels, namely: (i) radiative processes, (ii) ''reversible'' intramolecular radiationless processes, (iii) ''irreversible'' intramolecular radiationless processes, and (iv) collision-induced relaxation processes. Their respective dynamics may be investigated in a more detailed way, if the respective excited state is sensitive to external magnetic or electric fields. Both magnetic and electric fields induce small perturbations, which, however, may significantly change the excited-state dynamics.

It is well known [1] that perturbations induced by external magnetic and electric fields may be described by the respective Zeeman and Stark operators:

$$H_H(B) = -\mu_B[\vec{B}^{(s1)} \cdot (\overrightarrow{\mu_L}^{(s1)} + \overrightarrow{\mu_S}^{(s1)})] \tag{1}$$

$$H_{El}(E) = -(\vec{E}^{(s1)} \cdot \overrightarrow{\mu_{dip}}^{(s1)}). \tag{2}$$

In the above equations, the $(s1)$ superscript reminds that the respective quantities are spherical tensors of the first order, defined in the laboratory reference frame. In the well-known classical Zeeman, Hanle, and Stark effects, the observed phenomena are caused by field-induced level splitting of the respective states. In the magnetic field, the diagonal matrix elements of operator (1) are usually nonvanishing already in the first order of the perturbation theory. On the other hand, the diagonal matrix elements of electric-field operator (2) vanish in the first order of the perturbation theory in systems with an inversion centrum, but not in systems without this symmetry element. Additionally, level splitting due to the Zeeman and Stark effects induces polarization phenomena in luminescence. These effects have been studied extensively [2,3]. Our present attention will be thus focused on the less-studied phenomena, dependent on the off-diagonal matrix elements of both operators (1) and (2). Magnetic-field influence on the excited-state dynamics has already been documented for quite a few molecular systems [4–10]. The results were interpreted using various models: the level anticrossing effect theory; the direct mechanism theory, based on the magnetic-field-induced interaction between the levels of optically observable and ''dark'' states, arising in the first order of the perturbation theory; and the indirect mechanism theory, based on the magnetic-field-induced interaction between the levels of optically observable and ''dark'' states, arising in the second and higher orders of the perturbation theory. Typically, the indirect mechanism responsible for the S-T conversion dynamics may be detailed as the electron-spin and nuclear-spin decoupling mechanism (ESNSDCM). A famous case of the electric-field effect, which has been widely discussed [11], is the electric-field-induced mixing of the degenerate $2s$ and $2p$ states of the hydrogen atom. Since the symmetry of both the ground $1s$ state and the excited $2s$ state is ''g,'' an optical transition between these states is forbidden in the electric dipole approximation, remaining allowed between the $1s$ and the $2p$ ''u'' states. An external electric field mixes the $2s$ and $2p$ states in the first order of the perturbation theory. Thus, an exponential excited-state decay is observed in the absence of electric field, while in nonzero electric fields, quantum beats phenomena will be observed in collisionless conditions. The symmetries with respect to the inversion of the $\overrightarrow{\mu_L}^{(s1)} + \overrightarrow{\mu_S}^{(s1)}$ and $\overrightarrow{\mu_{dip}}^{(s1)}$ operators are ''g'' and ''u,'' respectively, therefore magnetic and electric fields should affect different channels of the excited-state evolution. The present paper is devoted to the acetylene molecule. This molecule has an inversion centrum ($D_{\infty h}$ point group in the ground state, and C_{2h} point group in the first excited electronic state) and is well studied as regards the influence of external magnetic and electric fields on its $\tilde{A}^1A_u$ excited-state dynamics.

TABLE I. Selected molecular parameter values for C_2H_2.

Parameter	Value
a'' (μs^{-1})	2.98 ± 0.13
b'' (μs^{-1} kV^{-2} cm^2)	$(4.87 \pm 0.09) \times 10^{-3}$
$\lvert C_{nS}\rvert^2$	9.6×10^{-4}
$\Sigma_T \lvert C_{nT}\rvert^2$	0.999
k_h (ms^{-1} $mTorr^{-1}$)	1.668 ± 0.011
k_l (s^{-1} $mTorr^{-1}$)	0.603 ± 0.007
D_0 (s^{-1} cm^{-2} $mTorr^{-1}$)	1.7
$V_1^2K_1^0$ [(band head)/cm^{-1}]	43 663.58 [13]
$V_1^2K_1^1$ [(band head)/cm^{-1}]	43 677.65 [13]
$V_1^2K_1^2$ [(band head)/cm^{-1}]	43 719.71 [13]
E_{dis}, (cm^{-1})	$43\,933.3 \pm 166.7$ [18]

The magnetic-field effects have been interpreted using the ESNSDCM theory [9,10], while the nature of the electric-field effects has not been understood by the previous authors [12].

We shall be discussing the $V_1^2K_1^{l=0,1,2}$ subbands of the acetylene laser-induced fluorescence (LIF) spectrum (Table I). These subbands belong to the $\tilde{A}\,^1A_u \rightarrow \tilde{X}^1\Sigma_g^+$ electronic transition [13,14]. The energies of the $V^2K^{l=0,1,2}$ levels lie below the dissociative threshold of the ground-state molecule [13,14]. Magnetic-field fluorescence quenching for these subbands is caused by collisions [9,10]. Thus, in the collisionless conditions, the only parameter of the acetylene fluorescence affected by the magnetic field is the decay lifetime: the signal amplitude is reduced, while the decay lifetime is increased, with the fluorescence quantum yield remaining constant. As we already noted, the magnetic-field effects were interpreted using the ESNSDCM theory, which predicts that the magnetic field affects the S-T conversion efficiency. Given that only the high-lying levels of the $\tilde{X}\,^1\Sigma_g^+$ singlet electronic ground state may get in the quasiresonance with the levels of the excited state of interest, magnetic field cannot induce the $S_1 \rightarrow S_0$ transition, as the respective matrix elements of operator (1) vanish due to symmetry rules: $\langle u|g|g\rangle = 0$. However, the matrix elements of operator (2) are nonvanishing: $\langle u|u|g\rangle \neq 0$, thus an external electric field should create a $S_1 \rightarrow S_0$ relaxation channel. Note that for both operators (1) and (2), the $\Delta S = 0$ selection rule is valid: see Refs. [9,10] for operator (1); the proof for operator (2) will be given later (see Sec. IV B); here S represents the total spin angular momentum.

In the present work, we studied the influence of an external electric field on the state dynamics of the acetylene molecule excited to specific rotational levels of the $V^2K^{l=0,1,2}$ vibronic states in the collisionless molecular-beam environment and in the bulk conditions. acetylene fluorescence kinetics and the IR emission integrated over the 833–1250 cm^{-1} spectral range were studied both in the absence and in the presence of magnetic and electric fields. Theoretical models explaining the observed electric-field effects and the IR emission kinetics have been proposed.

II. EXPERIMENT

An experimental setup used to study magnetic- and microwave-field effects on gas fluorescence has been described recently [15]. The present study used the same experimental setup, with the microwave cavity replaced by two electrodes, separated by 1 cm. The electric-field strength in the work zone was continuously variable from 0 to 30 kV/cm. Magnetic fields of up to 0.60 T were provided by an electromagnet, with additional coils for field zeroing and fine control. Magnetic-field strength was measured to better than 0.1 mT. Molecular jet exiting the pulsed electromagnetic valve was collimated by a skimmer. The valve nozzle was 0.1 mm in diameter; the distance from the nozzle to the skimmer inlet was 20 mm; the distance from the nozzle to the work zone was 70 mm. The laser beam, normal to the electric-field direction, passed through quartz windows. Fluorescence was observed in the direction normal to both the molecular beam and the excitation laser beam. It was collected by a telescope lens system and focused onto a Hamamatsu-R928 photomultiplier cathode through a long-pass filter, $\lambda > 285$ nm. The photomultiplier was perpendicular to both the electric-field direction and the excitation laser beam.

Excitation was provided by a frequency-doubled dye laser (λ-Physics, LPD-3000), with a BBO (barium-borate crystal) crystal for frequency doubling. Coumarin-47 dye (Surelite II) was used in the dye laser, pumped by a XeCl-excimer laser (λ-Physics, LPX-200). The spectral width, pulse duration, laser beam diameter, and pulse energy of the frequency-doubled dye laser radiation were $0.1-0.2$ cm^{-1}, $25-30$ ns, $2-3$ mm, and $7-10$ mJ, respectively, and the spectral interval covered ranged from 43 550 to 43 740 cm^{-1}. Pulse repetition rate of 5 Hz was used.

Total IR emission in the 833–1250 cm^{-1} spectral range was collected by a system of spherical mirrors with the reflection efficiency of about 99.5% in the spectral range of interest, and detected by a SiGe detector cooled to 77 K.

Data acquisition was controlled by an IBM PC Pentium III microcomputer, connected to a LeCroy 9450 digital oscilloscope via a GPIB interface (NI-488.2). The ScopExplorer software was used to transfer the recorded wave forms to the PC. Time resolution of the registration system was 4 ns. Boxcar integrator and other devices were connected to the PC via a PCI I/O board (Keithley, KPCI-1800). The data-acquisition system and the experimental setup control were implemented using the LabView package. Emission data were normalized to the laser pulse energy. In the decay measurements, transients were recorded both with and without the sample, $I_{sam}(t)$ and $I_{bg}(t)$, respectively, with the fluorescence decay signal subsequently calculated as the difference: $I_{sig}(t) = I_{sam}(t) - I_{bg}(t)$.

Commercial C_2H_2 from Matheson Gas Products Inc. was used as received.

III. RESULTS

We recorded the laser-induced fluorescence excitation spectra of the $\tilde{A}^1A_u(3^2K_a^{l=0,1,2}) \leftarrow \tilde{X}\,^1\Sigma_g^+(4^1,\Pi)$ transitions

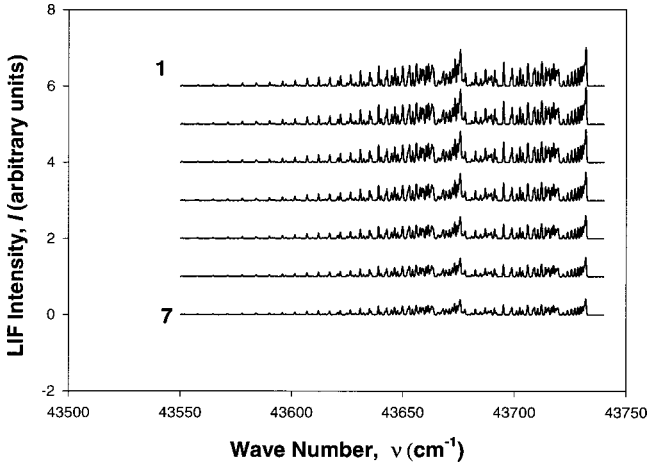

FIG. 1. Electric-field dependence of the LIF spectrum of acetylene recorded at $P=20$ mTorr for the $V_1^2K_1^{l=0,1,2}$ subbands of the $\tilde{A}^1A_u \leftarrow \tilde{X}\,^1\Sigma_g^+$ electronic transition. Spectra 1 to 7 correspond to $E=0$, 5, 10, 15, 20, 25, and 30 kV cm^{-1}, respectively.

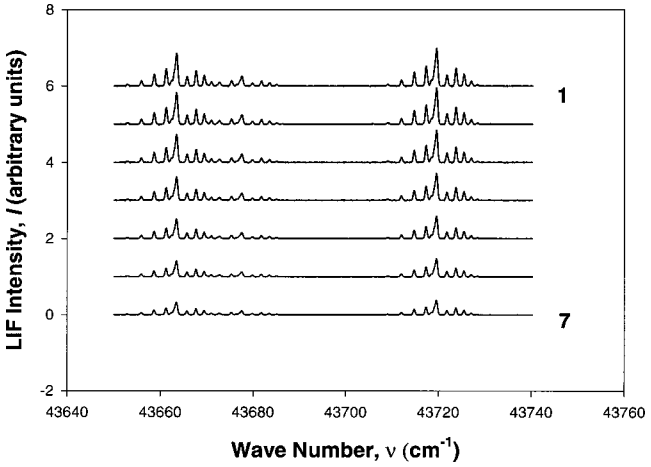

FIG. 2. Electric-field dependence of the LIF spectrum of acetylene recorded in the molecular beam: $P_0=1.7$ atm (Ar:acetylene $=95{:}5$) for the $V_1^2K_1^{l=0,1,2}$ subbands of the $\tilde{A}^1A_u \leftarrow \tilde{X}\,^1\Sigma_g^+$ electronic transition. Spectra 1 to 7 correspond to $E=0$, 5, 10, 15, 20, 25, and 30 kV cm^{-1}, respectively.

in acetylene in bulk and molecular-beam conditions in the presence of external electric fields of variable strength. Note that the spectral intensity dependence on the electric field was the same for the total intensity and for the individual rotational spectral components. Thus, we shall only discuss in detail the representative spectral transitions from the $\tilde{A}^1A_u(3^2K_a^2, J'=3)$ level. Electric-field dependences were also recorded for the fluorescence decay from the same level in the molecular-beam conditions. Finally, we studied the magnetic- and electric-field influence on the IR emission dynamics. Note that the IR emission was only recorded in the bulk conditions, in the presence of collision-induced phenomena.

A. Acetylene LIF spectra in electric fields

LIF spectra of the $V_1^2K_1^{l=0,1,2}$ subbands of acetylene were recorded in bulk conditions at $P=20$ mTorr in variable-strength electric fields, starting from zero. Typical spectra recorded are shown in Fig. 1. Note that the spectral intensities decrease at higher field strengths. Similar results were obtained in the molecular-beam conditions ($P_0=1.7$ atm, Ar:$C_2H_2=95{:}5$), with typical spectra shown in Fig. 2.

B. Field dependences

As was already noted, the field dependence was the same for the total LIF spectral intensity and for the individual rotational lines. Therefore, we shall only discuss such dependences for the $\tilde{A}^1A_u(3^2K_a^2, J'=3)$ level. The $[I(0)/I(E)-1]$ versus E^2 plots at $P=20$ mTorr (bulk conditions) and at $P_0=1.7$ atm, Ar:$C_2H_2=95{:}5$ (molecular-beam conditions) are presented in Figs. 3(a) and 3(b), respectively. Note that the experimental data may be fitted quite well by linear functions, where the respective slope b depends on pressure. Its value is higher for collisionless molecular-beam conditions as compared to the bulk conditions at $P=20$ mTorr. Accordingly, we proceeded to measure the pressure dependence of the b value.

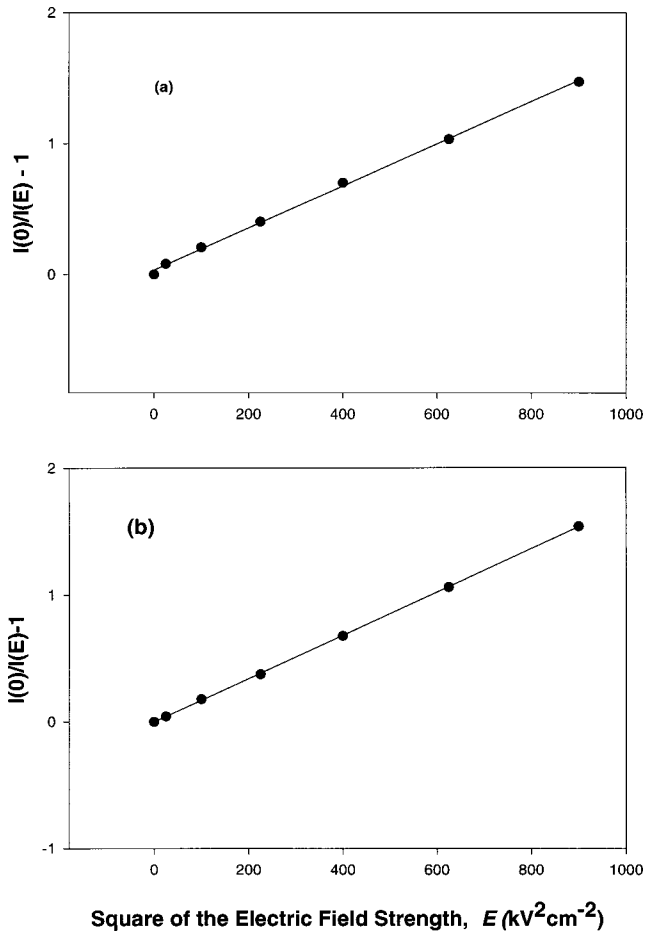

FIG. 3. The $[I(0)/I(E)-1]$ vs E^2 plot (a) at $P=20$ mTorr, the slope $b=1.61\times10^{-3}$ kV^2 cm^{-2}; (b) in the molecular beam: $P_0=1.7$ atm (Ar:acetylene$=95{:}5$), the slope $b=1.71\times10^{-3}$ kV^2 cm^{-2}. The data are presented for the $\tilde{A}^1A_u(3^2K_a^2, J'=3)$ level.

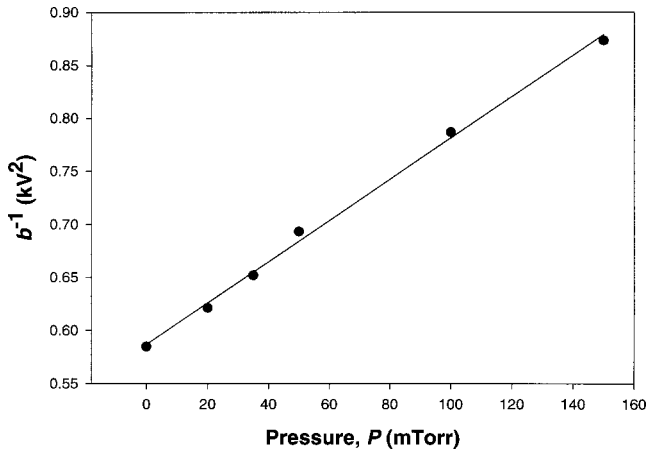

FIG. 4. The b^{-1} vs P linear plot presented for the $\tilde{A}^1A_u(3^2K_a^2,J'=3)$ level, intercept and slope are (0.59 ± 0.03) kV^2 cm^{-2} and $(1.95\pm0.07)\times10^{-3}$ kV^2 cm^{-2} mTorr^{-1}, respectively.

C. Pressure dependence of *b*

The b^{-1} versus P plot is shown in Fig. 4, and may be fitted by a linear function, with the values of intercept and slope of (0.59 ± 0.03) kV^2 cm^{-2} and $(1.95\pm0.07)\times10^{-3}$ kV^2/cm^{-2} mTorr^{-1}, respectively. These experimental results will be analyzed later.

D. Decay kinetics

Time-resolved measurements were carried out in the molecular-beam conditions at $P_0=1.7$ atm, Ar:C_2H_2 $=95:5$. The fluorescence decays measured for the $\tilde{A}^1A_u(V_1^2K_1^2,J'=3\leftarrow J''=2)$ line are shown in Fig. 5. Note that (i) the observed signal can be fitted with good accuracy by a single-exponential function,

$$I_{fl}(t)=A_0\exp\left(-\frac{t}{\tau_{fl}(E)}\right), \tag{3}$$

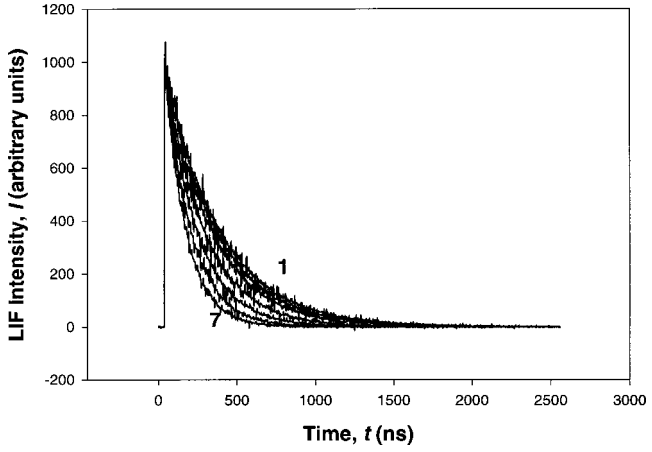

FIG. 5. Fluorescence decay dependence on the electric field strength measured in the molecular beam: $P_0=1.7$ atm (Ar:acetylene$=95:5$), the $\tilde{A}^1A_u(3^2K_a^2,J'=3)$ level. Decays 1 to 7 correspond to $E=0$, 5, 10, 15, 20, 25, and 30 kV cm^{-1}, respectively.

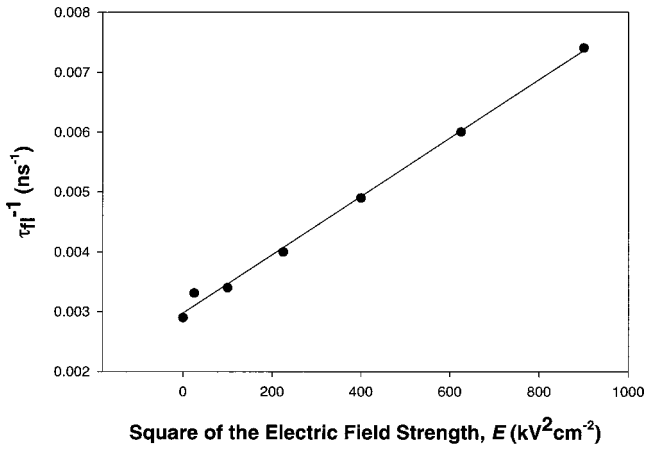

FIG. 6. The linear plot of $\tau_{fl}^{-1}(E)$ vs E^2, molecular beam: P_0 $=1.7$ atm (Ar:acetylene$=95:5$), the $\tilde{A}^1A_u(3^2K_a^2,J'=3)$ level.

and (ii) the decay lifetime decreases at increased field strength. Analysis of the $\tau_{fl}^{-1}(E)$ versus E^2 plot showed that this dependence may be fitted by a linear function [see Fig. 6(b)], whose intercept and slope values are (2.98 ± 0.13) μs^{-1} and $(4.87\pm0.09)10^{-3}$ μs^{-1}/kV^{-2} cm^2. The $\tau_{fl}(E)$ versus E plot is shown in Fig. 6(a) to demonstrate the effect studied. Note also that the signal amplitude is field independent. The field effect observed differs entirely from that due to magnetic-field influence on the acetylene fluorescence decay [9,10]. Namely, in presence of an external magnetic field the emission signal amplitude is reduced, with a simultaneous increase of the lifetime.

E. The IR emission measurements

Assuming that an external electric field induces transitions from the excited singlet-state levels to the quasiresonance levels of the ground state, the same electric field should induce IR emission due to radiative transitions between the ground-state vibrational levels. We have studied the IR emission dynamics in both electric and magnetic fields. Note that IR emission could only be observed in the bulk conditions. Typical IR emission kinetics at P $=20$ mTorr and without external fields is shown in Fig. 7(a). The initial section of the same trace is shown in Fig. 7(b). The observed decay kinetics may be fitted with good accuracy by a biexponential function,

$$I_{IR}(t)=A_0'\left[\exp\left(-\frac{t}{\tau_{IR,s}(0)}\right)-\exp\left(-\frac{t}{\tau_{IR,l}(0)}\right)\right], \tag{4}$$

where $\tau_{IR,s}(0)$ and $\tau_{IR,l}(0)$ are the IR emission lifetimes of the respective short- and long-lived components, in zero-field conditions. We have not detected any notable changes of the IR emission dynamics in the presence of external magnetic or electric fields. The observed emission intensity increase was in the 5–7 % range, which is close to the present experimental accuracy. These results will be discussed later.

Pressure dependence of the IR emission kinetics was studied in the 20–150 mTorr pressure range. The $\tau_{IR,s}(0)$ and $\tau_{IR,l}(0)$ parameter values were determined, and their pres-

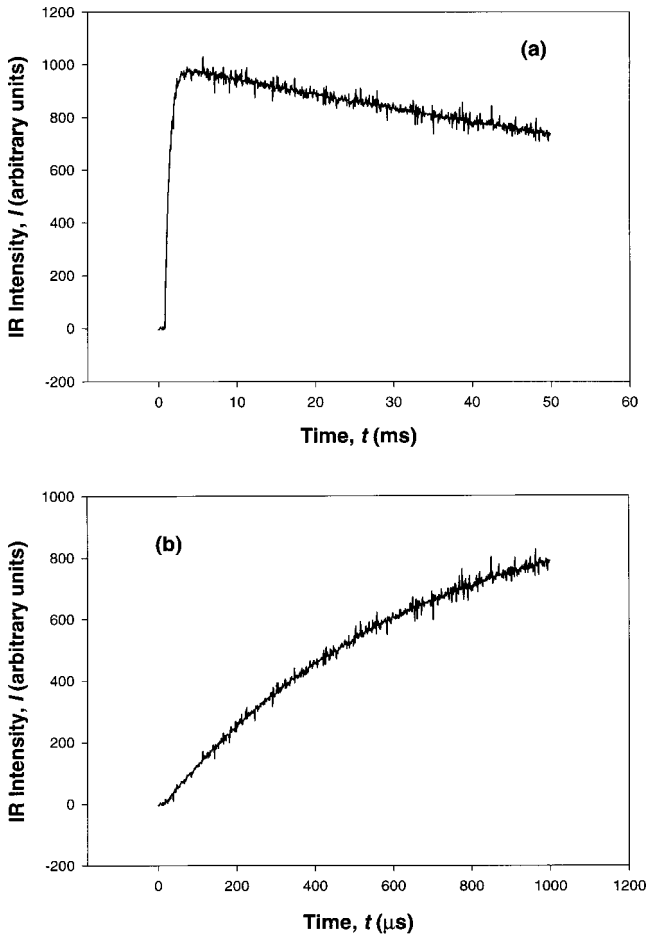

FIG. 7. (a) IR signal kinetics in the complete time range studied; (b) initial section. Measured at $P=20$ mTorr, acetylene excited to the $\tilde{A}^1A_u(3^2K_a^2, J'=3)$ level.

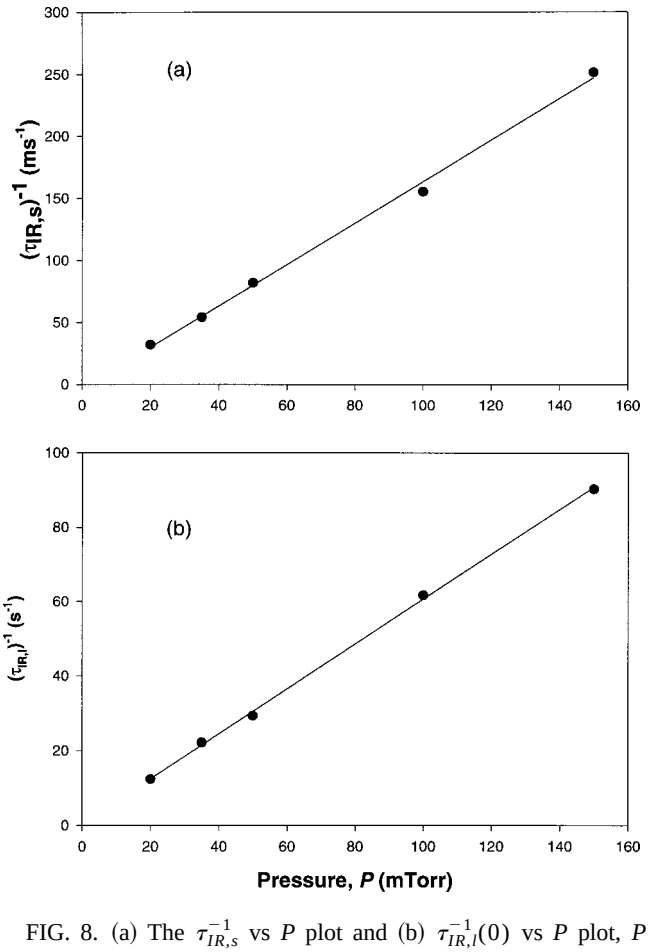

FIG. 8. (a) The $\tau_{IR,s}^{-1}$ vs P plot and (b) $\tau_{IR,l}^{-1}(0)$ vs P plot, $P=20$ mTorr, acetylene excited to the $\tilde{A}^1A_u(3^2K_a^2, J'=3)$ level.

sure dependence analyzed. The corresponding pressure plots are shown in Figs. 8(a) and 8(b); they were fitted by linear functions, with the slope values of (1.668 ± 0.011) $ms^{-1}\,mTorr^{-1}$ and (0.603 ± 0.007) $s^{-1}\,mTorr^{-1}$, for the respective short- and long-lived components.

IV. DATA ANALYSIS AND DISCUSSION

A. Qualitative interpretation

The effects observed may be interpreted in the framework of the radiationless transition theory. We shall assume that in acetylene an external electric field couples the levels of the $\tilde{A}\,^1A_u$ excited state to the ''quasiresonance'' levels of the $\tilde{X}\,^1\Sigma_g^+$ ground state. The proposed level scheme is shown in Fig. 9. It shows the levels of the $\tilde{A}^1A_u$ excited state coupled by the V_{ST} (spin orbit, vibronic spin orbit, or rotation spin orbit) and V_{SX}^0 (nonadiabatic or Coriolis) intramolecular interactions to the quasiresonance triplet- and ground-state levels, respectively. Note that the quasiresonance triplet levels in the energy range of interest belong to one of at least three different triplet states, denoted as $\tilde{a}^3B_u$, $\tilde{b}^3A_u$, and $\tilde{c}^3B_u$, whose nature will not be explored any further. An external electric field induces additional coupling between the excited

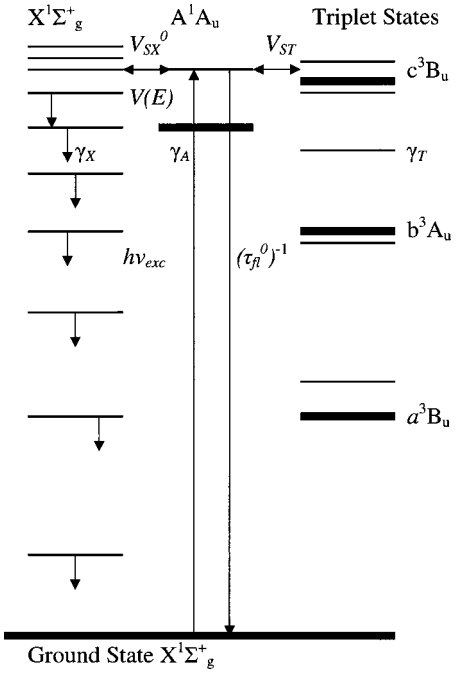

FIG. 9. Schematic representation of the electric field-induced quenching effect of the acetylene fluorescence.

singlet level and the quasiresonance ground-state levels, creating an additional radiationless channel for the excited-state relaxation. Since we assume that an external electric field induces the $S_1 \rightarrow S_0$ transition, then within the simplest kinetic scheme, the field dependence of the fluorescence quantum yield is given by $\phi_{fl}(E)=(\tau_{fl}^0)^{-1}/(\gamma_S+k_{SX}^0+k(E))$, where τ_{fl}^0 is the radiative lifetime of the excited level, $\gamma_S=(\tau_{fl}^0)^{-1}+k_qP$ is the width of the singlet levels studied (k_q is the collision-induced relaxation rate constant, P is the gas pressure), k_{SX}^0 is the rate constant of radiationless intramolecular $S_1 \rightarrow S_0$ transition, and $k(E)$ is the rate constant of field-induced radiationless $S_1 \rightarrow S_0$ transition. We shall discuss the physical meaning of these parameters later. Now, we shall only note that the emission quantum yield will decrease with growing electric-field strength, in accord with the experimental results: for instance, $\phi_{fl}(E)$ will decrease by a factor of 2 when $k(E)=\gamma_S+k_{SX}^0$. We are now passing to a theory that interprets the experimental behavior of the $k(E)$ rate constant.

B. General theory of the electric-field effect

We need to calculate the matrix elements of the Stark Hamiltonian:

$$H_{El}(E)=-(\vec{E}^{(s1)}\cdot\overrightarrow{\mu_{dip}}^{(s1)})=-\sum_{\substack{x,y,z\\ i=-1}}^{+1}(-1)^i(\vec{E}_i^{(s1)}\cdot\overrightarrow{\mu_{dip,i}}^{(s1)}), \tag{5}$$

where $\vec{E}^{(s1)}$ and $\overrightarrow{\mu_{dip}}^{(s1)}$ are the spherical tensor operators of the electric field and the electric dipole moment, defined in the laboratory frame of reference. For $\vec{E}^{(s1)}$ directed along the ''z'' axis of the laboratory frame of reference, Eq. (5) yields

$$H_{El}(E)=-E_z^{(s1)}\mu_{dip,z}^{(s1)}. \tag{6}$$

Since the electric dipole moment is coupled to the molecular reference frame, the z component of the dipole moment in Eq. (6) should be transformed to the molecular reference frame, thus Eq. (6) yields

$$\begin{aligned}H_{El}(E)&=-(E_z\mu_{dip,z}^{(s1)})\\&=-|E|\sum_{a,b,c,d}(1a,0c|10)(1b,1d|00)\\&\quad\times[D_{ab}^{(1)}(\omega)\mu_{dip,d}^{(1)}]\\&=-|E|\sum_q(10,00|10)(1q,1-q|00)\\&\quad\times[D_{0q}^{(1)}(\omega)\mu_{dip,-q}^{(1)}]\\&=-\frac{|E|}{\sqrt{3}}\sum_q(-1)^q[D_{0q}^{(1)}(\omega)\mu_{dip,-q}^{(1)}]\end{aligned} \tag{7}$$

as $a=c=0$ and $b=-d=q$. Here, $(ij,km|fl)$ is the Klebsch-Gordan coefficient, a,c,b,d are parameters determining this coefficient, $q=-1,0,+1$, $D(\omega)$ is the Euler rotation matrix, and $\mu^{(1)}$ the spherical tensor of the dipole moment operator defined in the molecular frame of reference. Thus the matrix elements of Eq. (7) may be represented in the form

$$\begin{aligned}&\langle\epsilon,v,J,N,K,M,S|H_Z(E)|\epsilon',v',J',N',K',M',S'\rangle\\&=-\frac{|E|}{\sqrt{3}}\sum_q(-1)^q\langle\epsilon,v,J,N,K,M,S|[D_{0q}^{(1)}(\omega)\mu_{dip,-q}^{(1)}]\\&\quad\times|\epsilon',v',J',N',K',M',S'\rangle\\&=-\frac{|E|}{\sqrt{3}}\sum_q(-1)^{q+M-K}[(2J+1)(2J'+1)]^{1/2}\\&\quad\times\begin{pmatrix}J&1&J'\\M&0&M'\end{pmatrix}\begin{pmatrix}J&1&J'\\K&q&K'\end{pmatrix}\langle\epsilon|\mu_{dip,-q}^{(1)}|\epsilon'\rangle\\&\quad\times\langle v|v'\rangle\delta_{SS'},\end{aligned} \tag{8}$$

where $\binom{ifk}{jlm}$ are the Wigner's coefficients, $q=-1,0,1$; ϵ are the quantum numbers defining the electronic state considered, v are the quantum numbers defining the vibrational state, J represents the total angular momentum, $N=R+L+l$ (R, L, and l being the respective rotational, electronic, and vibrational angular momenta), K is the projection of N on the axis of the molecular reference frame, M is the projection of J in the laboratory reference frame, and S is the spin angular momentum. It follows from the last equation that the matrix elements are nonvanishing if $\Delta J=0,\pm1$; $\Delta M=0$; $\Delta K=0,\pm1$; $\Delta S=0$. Note also that for $\epsilon=\epsilon'$ it follows that $\langle v|v'\rangle=\delta_{vv'}$, provided we only take into account the interaction of an external electric field with the electric dipole moment. The selection rules obtained coincide with the usual selection rules for the electric-dipole electronic transitions [16]. Note, however, that the physical nature of the phenomena is entirely different, as here we are considering quasiresonance transitions induced by a constant external electric field between levels of an optically observable and a ''dark'' state. For the acetylene molecule, only the $\langle\tilde{X}\,^1\Sigma_g^+|\mu_{dip,-q}^{(1)}|\tilde{A}\,^1A_u\rangle$ matrix elements have to be considered, between its fundamental S_0 and excited S_1 electronic state. The irreducible representation Σ_g^+ of the $D_{\infty h}$ point group correlates to the A_g irreducible representation of the C_{2h} point group. Within the C_{2h} point group, components of the $\mu_{dip,-q}^{(1)}$ spherical tensor are transformed by the $A_u(z;c)$ and $B_u(x,y;a,b)$ irreducible representations. Here both the xyz and abc coordinate systems are coupled to the molecular frame of reference, the first pertaining to the symmetry operators of the C_{2h} point group, and the second corresponding to the symmetric top axes. Since only the $\langle\tilde{X}\,^1\Sigma_g^+|A_u|\tilde{A}\,^1A_u\rangle$ matrix elements are nonvanishing ($q=\pm1$), the remaining selection rules in acetylene are $\Delta J=0,\pm1$; $\Delta K=\pm1$.

C. Theoretical interpretation of the electric-field effect

Noting that the electric field creates coupling between levels of the S_1 and S_0 states, and the vibrational level density of the ground state in the energy range considered is very high, $\rho_{vib} \approx 6 \times 10^3$ cm^{-1}, we assume that the electric-field-induced transition is irreversible, and its rate is described by the golden Fermi rule,

$$k_{nr}(E) = \frac{2\pi}{h} \rho_{vib} |V(E)|^2 = \alpha_{el} E^2. \tag{9}$$

As we see, the field-induced rate constant is proportional to the E^2 value. In the simplest case, the fluorescence quantum yield is given by

$$\phi_{fl}(E) = \frac{(\tau_{fl}^0)^{-1}}{\gamma_{ST}(E)}, \tag{10}$$

where τ_{fl}^0 is the radiative lifetime of the unperturbed singlet levels, and

$$\gamma_{ST}(E) = |C_{nS}|^2 \gamma_S(E) + \sum_T |C_{nT}|^2 \gamma_T \tag{11}$$

because the singlet levels considered are also coupled by the S-T interaction to discrete levels of the adjacent triplet states [9,10]. Here,

$$\gamma_S(E) = (\tau_{fl}^0)^{-1} + k_{q,S} P + k_{nr}^0 + k_{nr}(E) \tag{12}$$

and

$$\gamma_T(E) = k_{q,T} P + k_{nr,T}^0, \tag{13}$$

where

$$k_{nr}^0 = \frac{2\pi}{h} \rho_{vib} |V_{SX}^0|^2, \tag{14}$$

$$k_{nr,T}^0 = \frac{2\pi}{h} \rho_{vib} |V_{TX}^0|^2 \tag{15}$$

are the radiationless rate constants; and $k_{q,S}$ and $k_{q,T}$ are the rate constants of collision-induced relaxation, of the respective singlet and triplet levels. It has been shown [10] that for triplet levels coupled to the singlet levels of interest, $k_{nr,T}^0 = 0$ with good accuracy.

In our experiments, the $\delta_{fl}(E) = \phi_{fl}(0)/\phi_{fl}(E) - 1$ and $\gamma_{ST}(E)$ plots versus E^2 were analyzed, and both were found to be linear. This result directly follows from the equations presented above. For the first plot, the slope value is given by

$$b = \frac{\alpha_{el}}{\gamma_{ST}(0)}, \tag{16}$$

where b^{-1} should be linear on the sample pressure. Experimental results confirm such a linear dependence, wherein the respective intercept and slope are given by

$$a' = |C_{nS}|^2 \frac{[(\tau_{fl}^0)^{-1} + k_{nr}^0]}{\alpha_{el}}, \tag{17}$$

$$b' = |C_{nS}|^2 \frac{k_{q,S}}{\alpha_{el}} + \frac{\sum_T |C_{nT}|^2 k_{q,T}}{\alpha_{el}}. \tag{18}$$

Since $\gamma_{ST}(E)$ was measured in the molecular beam (collisionless conditions), the intercept and slope values of the $\gamma_{ST}(E)$ versus E^2 plot are simply given by

$$a'' = (\tau_{fl}^0)^{-1} + k_{nr}^0 \approx (2.98 \pm 0.13)\ \mu\text{s}^{-1}, \tag{19}$$

$$b'' = \alpha_{el} \approx (4.87 \pm 0.09) \times 10^{-3}\ \ \mu\text{s}^{-1}\ \text{kV}^{-2}\,\text{cm}^2. \tag{20}$$

The parameter values obtained for the field-free case are in good agreement with the previously published results [9,10]. Thus, the presently proposed theoretical model correctly describes the experimentally observed electric-field effects. Using the a'', b'', and Eq. (17) and the relation $\Sigma_T |C_{nT}|^2 = 1 - |C_{nS}|^2$, we calculated the $|C_{nS}|^2$ and $\Sigma_T |C_{nT}|^2$ parameters. These results are presented in the Table I along with the a'' and b'' values.

D. IR emission results

We found that the IR emission in the 833–1250 cm^{-1} spectral range is collision induced, same as its quenching. The observed effects may be understood assuming the existence of an efficient radiationless transition channel from the levels of the S_1 state to the highly lying rovibronic levels of the S_0 state, which translates into high values of the k_{nr}^0 rate constant. This hypothesis is consistent with the low absolute fluorescence quantum yield value of 0.13 [17], which may thus result from irreversible radiationless relaxation to the S_0 levels. This would additionally explain the small field effect values in the IR emission, which could not be measured reliably, as their expected values are only about 7% of the IR emission intensity.

Given the very high level densities of the ground state in the spectral range considered, and noting that the transition rate constant from the S_0 spectrum to the S_1 levels is equally proportional to ρ_{vib}^{-1}, we can use the collisionless approximation for the irreversible radiationless transitions to the S_0 levels in the time range of interest. This approximation is valid in the molecular-beam conditions, with the molecule surviving longer in the highly excited vibronic levels of the ground state. In the bulk conditions, we must additionally account for the collision-induced processes within the ground-state vibrational spectrum. Dynamics of the relaxation processes within the S_0 spectrum is very complex, and cannot be analyzed exactly. We shall use two approximate approaches to the calculations: (i) a simple kinetic model, and (ii) an ''energy diffusion'' model, considering the system diffusion within the energy spectrum of the ground state. The first approach uses certain average kinetic parameters, the values of which can be extracted from experimental results. The second approach considers the collision-induced relaxation process over the ground-state energy spectrum as a

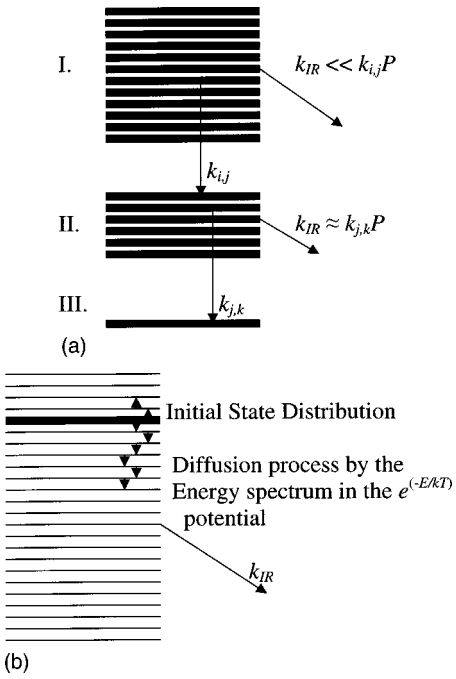

FIG. 10. (a) Schematic representation of the simplest kinetics model, and (b) diffusion model in the energy space used to analyze the IR signal dynamics.

diffusion process, whereby the initially prepared state distribution evolves within the energy spectrum of the ground state in the presence of the Boltzmann potential.

1. Simple kinetic model

The model is schematically represented in Figs. 10(a). In the framework of this model, we shall separate the S_0 energy spectrum in three parts: $\langle h|$—the highly excited S_0 levels, with undetectably low yields of IR emission; $\langle l|$—the excited levels, for which the IR emission is detectable, and $\langle g|$—the vibrationless ground state, to which the system will eventually relax. We shall assume that transitions from the $\langle h|$ levels to the $\langle l|$ levels are induced by collisions, k_h being the averaged transition rate constant; the transitions from the $\langle l|$ levels to the $\langle g|$ levels are also induced by collisions, k_l being the respective rate constant; and that the $\langle l|$ levels can also undergo radiational IR transitions, τ_{IR} being the respective lifetime:

$$\langle h| \xrightarrow{k_h} \langle l|,$$

$$\langle l| \xrightarrow{k_l} \langle g|,$$

$$\langle l| \xrightarrow{(\tau_{IR})^{-1}} \langle g| + h\nu.$$

The IR emission kinetics in this model has the functional form identical to that of the experimental results

$$I_{IR}(t) = \frac{C_0}{k_h P - (\tau_{IR})^{-1} - k_l P} (\exp\{-[(\tau_{IR})^{-1} + k_l P]t\} - \exp(-k_h P t)). \tag{21}$$

The k_h and k_l values presented in Table I were chosen to obtain the best fit to the data. This model is in qualitative agreement with the general theory of the collision-induced relaxation processes, in that the efficiency of the collision-induced relaxation increases with the level density (see Appendix A).

2. Energy diffusion model

A schematic representation of this model is shown in Figs. 10(b). In the frameworks of this model, the time evolution of the initially prepared state may be described by diffusion of the state populations within the energy spectrum of the electronic state considered. The diffusion equation may be written as

$$\frac{\partial n(t,E)}{\partial t} = -D(E)\hat{L}n(t,E), \tag{22}$$

where $\hat{L}$ is the diffusion operator (see Appendix B), and $D(E)$ is a function of energy. Since the initially prepared state is a single rotational level, and the final population distribution is the Boltzmann function, the $n(t,E)$ function should satisfy the following initial and boundary conditions:

$$n(0,E) = n_0 \delta_{E_0 E}, \tag{23}$$

$$n(t,E) = 0, \quad E > E_0,$$

$$n(\infty,E) = n_0 \exp\left(-\frac{E}{kT}\right),$$

$$\int n(t,E)dE = n_0 = \text{const},$$

where E_0 is the excitation energy. According to Appendix A, the transition probability is proportional to the level density squared, thus the $D(E)$ function may be represented as

$$D(E) = D_0 n \frac{|V_{km}^{(0)}|^2}{h^2} \rho_k^2(E), \tag{24}$$

where D_0 is a constant and n the numerical density of the buffer gas molecules. Since the relation $\rho_{vib}(E) < \rho_{rot}(E) < \rho_{transl}(E)$ is satisfied, it is sufficient to consider the relaxation over the vibrational spectrum, which is the slowest process.

The IR intensity time dependence may be written as

$$I_{IR}(t) = \int_0^\infty \phi_{IR}(E) n(t,E) dE, \tag{25}$$

where

$$\phi_{IR}(E)=\frac{[\tau_{IR}(E)]^{-1}}{[\tau_{IR}(E)]^{-1}+\sigma_{vv'}(E)\overline{vn}}. \tag{26}$$

Here, $\tau_{IR}(E)$ is the energy-dependent IR emission lifetime, $\sigma_{vv'}(E)$ is defined in Appendix A, and $\overline{v}$ is the averaged relative molecular velocity. To simplify this expression, let us assume that the energy dependence of $\tau_{IR}(E)$ is negligible, so that an averaged value $\overline{\tau_{IR}}$ may be used instead. Typical values of the IR emission lifetimes of polyatomic molecules are in the millisecond time range. Thus, we shall use the IR radiative constant of 10^3 s^{-1} in our estimates. Using the maximum of the Lennard-Jones interaction potential for the acetylene molecule in the ground electronic state, and determining the normalized transition probability, the energy-dependent values were estimated as follows: $\sigma_{vv'}(E)=10^{-52}E^{12}$ cm^2 and $D(E)=10^{-52}D_0nE^{12}$ s^{-1} cm^{-2}. Now, Eq. (22) can be solved, and the D_0 parameter estimated, using the experimental data. After determining the D_0 value and finding the $n(t,E)$ function, the relaxation dynamics of the studied system over the ground-state spectrum will be fully known. Hence, we shall know the time evolution of the state populations, and thus will be able to calculate any energy-dependent physical value $f(E)$ in our system, by averaging over the energy distribution,

$$\overline{f(t)}=\frac{\int f(E)n(t,E)dE}{\int n(t,E)dE}. \tag{27}$$

Since the $\tau_{IR,s}^{-1}(0)$ versus P and $\tau_{IR,l}^{-1}(0)$ versus P plots are linear, we can try to estimate the D_0 value using Eqs. (24) and (26). The slope values of these plots will be approximately given by $10^{-52}D_0\overline{E_s^{12}}$ and $10^{-52}D_0\overline{E_l^{12}}$, where

$$\overline{E_q^{12}}=\frac{E_{q1}^{13}-E_{q2}^{13}}{13(E_{q1}-E_{q2})}, \quad q=s,l \tag{28}$$

is the averaged value for the respective short- and long-lived components of the IR emission. For the long-lived component, it is difficult to estimate the E_{l1} and E_{l2} values. However, we can make the required estimates for the short-lived component, assuming that E_{s2} corresponds to the relation $[\tau_{IR}(E)]^{-1}=0.1\sigma_{vv'}(E)\overline{vn}$, and thus use $E_{s2}\approx 1000$–2000 cm^{-1} and setting $E_{s1}=E_0$. Thus, we can calculate D_0, obtaining the value shown in the Table I. The estimates performed are very rough, but may be used to obtain qualitative conclusions.

Qualitatively, the energy diffusion process may be envisioned as a combined action of two factors. The first one, the random energy diffusion process, increases the width of the initial narrow state distribution. Note that since the level density increases with E, the diffusion rate is asymmetric, growing towards higher energies. The second factor, the directional drift in the Boltzmann potential, gradually shifts the distribution maximum towards the vibrationless state. Note that the two factors act in opposite directions, although eventually the Boltzmann potential defines the final state of the system.

In the present study, we have not solved Eq. (22) analytically. Its numerical analysis is presented in Appendix B. As is shown in Appendix B, the energy diffusion flux is described by two terms: (i) $\vec{\nabla}n(t,E)$—the random diffusion flux and (ii) $n(t,E)\vec{\nabla}\psi(E,T)$—the drift in the Boltzmann potential. The first term describes the energy diffusion process with equal probability in both directions, provided $D(E)$ is independent of E. However, with $D(E)$ being a growing function of E, the diffusion process should be faster towards higher energies. The second term describes the system drift in the Boltzmann potential: $\psi(E,T)=\exp[-E/kT]$. The diffusion flux for this term is directed towards lower energies. As the system eventually achieves the Boltzmann distribution, we assume that the relation $\vec{\nabla}n(t,E)<n(t,E)\vec{\nabla}\psi(E,T)$ is satisfied everywhere and at all times. If, additionally, $\vec{\nabla}n(t,E)\ll n(t,E)\vec{\nabla}\psi(E,T)$ is satisfied, then the problem may be significantly simplified, and the solution obtained in the form

$$n(t,E)=n_0(E)\exp\left[-\frac{D(E)\exp\left(\frac{E}{kT}\right)}{(kT)^2}t\right]. \tag{29}$$

Here, the $n_0(E)$ function is unknown, and has to be found using the mass balance condition,

$$\int n(t,E)dE=\int n_0(E)\exp\left[-\frac{D(E)\exp\left(\frac{E}{kT}\right)}{(kT)^2}t\right]dE=n_0 = \text{const} \tag{30}$$

—this integral should be constant. We leave the detailed analysis of this approximation for another occasion.

Finally, we list the most important molecular parameters of acetylene estimated in our calculations

V. CONCLUSIONS

We have studied acetylene fluorescence quenching induced by an external electric field. The external electric field induces an additional radiationless transition channel to the ground-state levels, coupling levels of the $\tilde{A}\,^1A_u$ excited state to the quasiresonance levels of the $\tilde{X}\,^1\Sigma_g^+$ ground state. As the level density of the ground state in the vicinity of the excited state is very high, the electric-field-induced transition may be considered irreversible, with the rate constant described by the Fermi rule. A phenomenological kinetic model based on this rate constant estimate was used to analyze the experimental data obtained, and the field-induced relaxation rate constant estimated. An electric field in this case can be used as an external small perturbation, which significantly changes the excited state dynamics of the studied system.

IR emission of the excited vibronic ground-state levels

was investigated for any indication of magnetic- or electric-field effects. No such effects were observed within the present experimental capabilities. These results were interpreted in the light of the previous work by Suzuki *et al.* [17], who found that the fluorescence quantum yield of acetylene into individual rotational levels of the band system studied is only about 0.13 at the collisionless conditions. Consequently, acetylene has an efficient natural radiationless relaxation channel from the electronically excited state to the ground state, even in zero fields. The observed IR emission dynamics was analyzed using a simple kinetic model and the spectral diffusion model. Some of the relevant model parameters have been estimated. The models proposed may be applied to the IR emission dynamics of highly excited vibronic levels of other molecules.

APPENDIX A: COLLISION-INDUCED RELAXATION

1. Introduction

A general case of collision-induced relaxation is considered: the excited singlet-state levels $|s\rangle$ are coupled by an intramolecular interaction to discrete levels $|q\rangle$ of a neighboring electronic state. The results obtained within this model are directly applicable to an unperturbed state. A mixed wave function $|n\rangle$ may thus be represented as

$$|n\rangle = C_{sn}|s\rangle + \sum_q C_{qn}|q\rangle. \tag{A1}$$

The width of the mixed states $|n\rangle$ is determined by

$$\Gamma_n = |C_{sn}|^2 \gamma_s + \sum_q |C_{qn}|^2 \gamma_q, \tag{A2}$$

where

$$\gamma_s = (\tau_{fl}^s)^{-1} + \sum_i \sigma_i^s n\overline{v}, \quad \gamma_q = (\tau_{IR}^q)^{-1} + \sum_i \sigma_i^q n\overline{v}, \tag{A3}$$

$$\sigma_i^s = \sigma_{ie}^s + \sigma_{iv}^s + \sigma_{ir}^s, \quad \sigma_i^q = \sigma_{ie}^q + \sigma_{iv}^q + \sigma_{ir}^q, \tag{A4}$$

$$\sigma_{ie}^s = \sum_{v',j'} \sigma_{ivj,v'j'}^{s,A-X}, \quad \sigma_{iv}^s = \sum_{v'\neq v,j'} \sigma_{ivj,v'j'}^{s,A},$$

$$\sigma_{ir}^s = \sum_{j'\neq j} \sigma_{ivj,vj'}^{s,A}, \tag{A5}$$

$$\sigma_{ie}^q = \sum_{v',j'} \sigma_{ivj,v'j'}^{q,X-A}, \quad \sigma_{iv}^q = \sum_{v'\neq v,j'} \sigma_{ivj,v'j'}^{q,X},$$

$$\sigma_{ir}^q = \sum_{j'\neq j} \sigma_{ivj,vj'}^{q,X}. \tag{A6}$$

Cross sections for various collision-induced relaxation processes are given by

$$\sigma_{i\epsilon vj,\epsilon' v' j'}^R = \sigma_{i0}(T) \int_{-\infty}^{+\infty} W_{\epsilon vj,\epsilon' v' j'}(t)\,dt, \tag{A7}$$

where

$$W_{\epsilon vj,\epsilon' v' j'} = |\langle \epsilon vj|\hat{V}(t)|\epsilon' v' j'\rangle|^2. \tag{A8}$$

Here, σ is the collision-induced cross section, the ''s'' and ''q'' are indices determining excited electronic singlet and neighboring ''dark'' state, the other indices determine the state considered—electronic, vibration, and rotation quantum numbers, τ_{fl}^s and τ_{IR}^q are radiative lifetimes of the acetylene fluorescence and IR emission of the ''dark'' state, n is the gas density, and $\overline{v}$ is the averaged relative velocity of molecules.

2. Simple model: *V-T* and *R-T* relaxation

We shall use the general approach of the time-dependent perturbation theory. In the framework of this theory, the Schrödinger equation is written as

$$ih\frac{\partial \Psi}{\partial t} = [\hat{H}_0 + \hat{V}(t)]\Psi, \tag{A9}$$

where the time-dependent wave function may be represented as

$$\Psi_n(t) = \sum_k a_{kn}(t)\psi_k. \tag{A10}$$

Here, each of the time-independent wave functions obeys the equation

$$ih\frac{\partial \psi_k}{\partial t} = \hat{H}_0 \psi_k. \tag{A11}$$

Thus,

$$ih\sum_k \psi_k \frac{\partial a_{kn}}{\partial t} = \sum_k a_{kn}\hat{V}(t)\psi_k, \tag{A12}$$

$$ih\frac{\partial a_{mn}}{\partial t} = \sum_k a_{kn} V_{mk}(t) e^{i\omega_{mk}t}, \tag{A13}$$

where the constants are determined as follows:

$$a_k = a_k^{(0)} + a_k^{(1)}, \quad a_m^{(0)} = 1, \quad a_k^{(0)} = 0, \quad k \neq m, \tag{A14}$$

$$ih\frac{\partial a_{kn}^{(1)}}{\partial t} = V_{kn}(t) e^{i\omega_{nk}t}, \tag{A15}$$

$$a_{kn}^{(1)} = -\frac{i}{h}\int_{-\infty}^{+\infty} V_{kn}(t) e^{i\omega_{nk}t}\,dt. \tag{A16}$$

In the first approximation

$$a_{km}^{(1)} = -\frac{i}{h}\int_{-\infty}^{+\infty} V_{km}(t) e^{i\omega_{km}t}\,dt, \tag{A17}$$

$$a_{mn}^{(1)}=1-\frac{i}{h}\int_{-\infty}^{+\infty}V_{mm}(t)dt, \tag{A18}$$

$$a_{kn}^{(1)}(-\infty)=0, \quad a_{kn}^{(1)}(+\infty)\neq 0, \tag{A19}$$

$$\Psi_n(\infty)=\sum_k a_{kn}(\infty)\psi_k, \tag{A20}$$

$$W_{kn}=|a_{kn}(\infty)|^2=\frac{1}{h^2}\left|\int_{-\infty}^{+\infty}V_{km}(t)e^{i\omega_{km}t}dt\right|^2, \tag{A21}$$

$$\frac{i}{h}\int_{-\infty}^{+\infty}V_{km}(t)e^{i\omega_{km}t}dt=-\left[\frac{V_{km}(t)e^{i\omega_{km}t}}{h\omega_{km}}\right]_{-\infty}^{t}+\int_{-\infty}^{t}\frac{\theta V_{km}(t)}{\partial t}\frac{e^{i\omega_{km}t}}{h\omega_{km}}dt. \tag{A22}$$

For a perturbation given by a rectangular pulse of the width τ:

$$V_{km}(t)=0, \quad -\infty<t<-\frac{\tau}{2}, \tag{A23}$$

$$V_{km}(t)=V_{km}^{(0)}, \quad -\frac{\tau}{2}\leqslant t\leqslant\frac{\tau}{2},$$

$$V_{km}(t)=0, \quad \frac{\tau}{2}<t<\infty,$$

we obtain

$$\begin{aligned}\frac{i}{h}\int_{-\infty}^{+\infty}V_{km}(t)e^{i\omega_{km}t}dt&=-\frac{V_{km}^{(0)}[e^{i\omega_{km}\tau/2}-e^{-i\omega_{km}\tau/2}]}{h\omega_{km}}+\int_{-\infty}^{t}\frac{\theta V_{km}(t)}{\partial t}\frac{e^{i\omega_{km}t}}{h\omega_{km}}dt\\&=-\frac{V_{km}^{(0)}2i\sin\left(\omega_{km}\frac{\tau}{2}\right)}{h\omega_{km}}+\int_{-\infty}^{t}\frac{\theta V_{km}(t)}{\partial t}\frac{e^{i\omega_{km}t}}{h\omega_{km}}dt\\&\approx-\frac{iV_{km}^{(0)}\tau}{h}+\int_{-\tau/2}^{\tau/2}\frac{\theta V_{km}(t)}{\partial t}\frac{e^{i\omega_{km}t}}{h\omega_{km}}dt.\end{aligned} \tag{A24}$$

For $|V_{km}^{(0)}\tau/h|\ll 1$, the integral of interest is given by the second term

$$\int_{-\tau/2}^{\tau/2}\frac{\theta V_{km}(t)}{\partial t}\frac{e^{i\omega_{km}t}}{h\omega_{km}}dt, \tag{A25}$$

thus

$$W_{kn}\approx\frac{1}{h^2\omega_{km}^2}\left|\int_{-\Delta\tau/2}^{\Delta\tau/2}\frac{\theta V_{km}(t)}{\partial t}e^{i\omega_{km}t}dt\right|^2\approx\frac{|V_{km}^{(0)}|^2}{h^2\omega_{km}^2}=\frac{|V_{km}^{(0)}|^2}{h^2}\rho_k^2(E). \tag{A26}$$

The densities of vibrational, rotational, and translational states are given by the usual expressions

$$\rho_{vib}(E_v)=\frac{[E_v+a\overline{\nu}_0]^{s-1}}{(s-1)!\prod_i\nu_i}, \tag{A27}$$

$$\rho_{rot}(E_r)=\frac{Q_r}{\Gamma\left(1+\frac{1}{2}r\right)}\left(\frac{E_r}{kT}\right)^{(1/2)r}, \tag{A28}$$

$$\rho_{trans}(E)=\left[\frac{2\pi kT}{h^2}\right]^{3/2}, \tag{A29}$$

where the rotational statistical sum is

$$Q_r=\prod_{i=1}^{p}\left[\left(\frac{8\pi^2I_ikT}{h^2}\right)^{(1/2)d_i}\Gamma\left(\frac{1}{2}d_i\right)\right]. \tag{A30}$$

Here, d_i is the degeneration degree of the respective rotation. The $V_{km}^{(0)}$ value may be determined using the maximum value of the Lennard-Jones potential for the colliding particles.

Note that the $v-v'$ energy transfer and the collision-complex-formation phenomena may also be described as collision-induced relaxation. Such energy-transfer phenomena may be analyzed using the dipole-dipole and contact interaction mechanisms. Presently, we shall disregard the relaxation due to energy transfer, although it can be very important for some of the levels, which happen to be in the ''quasiresonance'' with those of a colliding buffer molecule. Note that resonance energy transfer, whereby the entire excess energy is transferred to another molecule of the same nature, is not a relaxation process.

An additional relaxation pathway involves complex formation between the excited and buffer molecules. The complex lifetime should be longer than the rotation period of the system. A detailed treatment and analysis of this model has been performed previously [19]. In the framework of this model, the excess energy is redistributed between the initially excited and the buffer molecule during the complex lifetime, the energy redistribution rate being determined by the interactions between the components. One might expect, however, that the collision-complex lifetime will decrease towards increasing excess energy of the excited molecule. Hence, this mechanism should lose its importance in systems with high vibrational excitation, where the respective collision-complex lifetime becomes very short. Thus, we shall limit ourselves to the simple relaxation model presented above.

APPENDIX B

We shall describe in detail the energy diffusion model used. One of the reasons is that this problem of physical chemistry has immediate practical applications, notably for the important problem of atmospheric global warming, as the atmospheric energy redistribution processes are strongly dependent on the molecular energy relaxation phenomena under discussion.

Radiationless transitions from levels of electronically excited states to ''quasiresonance'' neighboring ''dark'' levels, which frequently belong to the ground state, take place in every polyatomic molecule. Thus, it becomes very important to study the vibrational energy transformation phenomena resulting in IR emission and in translational energy increase of molecules colliding with an excited molecule considered. Note that the efficiency of allowed electronic transitions is much higher than that of allowed vibrational transitions, resulting in much larger energies absorbed via UV and visible photons as compared to IR photons. Also, considering the UV-VIS spectral range, which corresponds to transition energies of 30 000–20 000 cm^{-1}, the respective excited molecule excess energy amounts to about $(100–150)kT$, while a typical vibrational transition corresponds to only about $(5–15)kT$. Here the value of kT was estimated at $T=300$ K; this value is only weakly dependent on height in the tropospheric layer, where the temperature stays within the 200 to 300 K range. Therefore, the mechanism discussed can decisively affect the primary energy redistribution pathways and thus play an important role in the atmospheric global warming. The state evolution dynamics discussed in this section has already been investigated for NO_2 [20], SO_2 [21], and CS_2 [22]. The results obtained, however, have never been applied to the problem presently considered. The quantities of fundamental importance are

$$e_1=\frac{\int\int\int \phi_{IR}(l,E)n(t,E,l)dEdtdl}{\int\int\int I_{exc}(t,\omega)\{1-\exp[-\sigma_{abs}(\omega)\ln(l)]\}d\omega dtdl} \tag{B1}$$

—the energy fraction transformed into the IR emission, about half of which is dissipated into the outer space, and the remaining part—absorbed by the Earth surface, and

$$e_2=\frac{\int\int\int n(t,E,l)[1-\phi_{IR}(l,E)]dEdtdl}{\int\int\int I_{exc}(t,\omega)\{1-\exp[-\sigma_{abs}(\omega)\ln(l)]\}d\omega dtdl} \tag{B2}$$

—the energy fraction transformed into the translational energy of molecules. Here, $\phi_{IR}(l,E)$ is the IR emission yield as a function of the energy excess, dependent also on the buffer gas pressure; $n(t,E,l)$ is the population distribution in the system over the energy spectrum of the ''dark'' state, $I_{exc}(t,\omega)$ is the spectral intensity distribution on the excitation radiation source, $\sigma_{abs}(\omega)$ is the absorption cross section of the system, l is the optical path length, and $n(l)$ is the density distribution of the molecules of interest. Generally, the $\phi_{IR}(l,E)$ and $n(t,E,l)$ functions are dependent on l, height above the surface. All these functions are implicitly dependent on the gas density, as the latter is dependent on l. The e_1 and e_2 values may be related directly to the problem discussed, although a lot of system parameters must be determined before the equations can be put to practical usage. In the present study, the dynamics of the IR emission of C_2H_2 was studied. The problem represented by Eqs. (B1) and (B2) consists of two independent parts, related to calculation of the respective $\phi_{IR}(l,E)$ and $n(t,E,l)$ functions. The latter function can be obtained by solving Eq. (22).

1. Numerical method of finite differences

The equation discussed is

$$\frac{\partial n(t,E)}{\partial t}=-D(E)\hat{L}n(t,E), \tag{B3}$$

where

$$D(E)\hat{L}n(t,E)=D(E)\vec{\nabla}\cdot\vec{j}. \tag{B4}$$

Here,

$$\vec{j}=(\vec{j}_1+\vec{j}_2)=\vec{\nabla}n(t,E)+n(t,E)\vec{\nabla}\psi(E,T), \tag{B5}$$

$$\vec{\nabla}=\frac{\vec{\partial}}{\partial E} \tag{B6}$$

and $\psi(E,T)$ is the Boltzmann potential. We shall use the finite-difference techniques to analyze the problem numerically [23].

a. Choice of the numerical grid

To build the numerical grid, Peterson and Freed [23] proposed to use the h_1 step up to a certain point ''i,'' $1\leqslant i<N$, and the $h_2>h_1$ step for the remaining interval, $i<j\leqslant N$. Such an approach significantly facilitates the construction of the finite-difference scheme, and is frequently used. However, this approach has some drawbacks, due to an unnecessary step reduction in the intermediate region. Besides, it has been shown that the finite-difference scheme loses its accuracy in the vicinity of a sharp transition from h_1 to h_2 [24].

An alternative approach includes mapping of the diffusion region onto an interval of ζ, such as $E=e(\zeta)$. The function $e(\zeta)$ is chosen such that passing the lower frontier, the step given by

$$h_i=E_{i+1}-E_i=e(\zeta_{i+1})-e(\zeta_i) \tag{B7}$$

will gradually become smaller than its initial high value h_1. The knots of the finite-difference scheme correspond to integer ζ values. If the relation

$$|h_{i+1}-h_i|\ll h_i \tag{B8}$$

is satisfied, that is,

$$\left|\frac{d^2e(\zeta)}{d\zeta^2}\right| \ll \left|\frac{de(\zeta)}{d\zeta}\right| \tag{B9}$$

then the respective grid is called quasiproportional [25]. Such grids allow to obtain a very good approximation of the original continuous differential equations. The choice of the $e(\zeta)$ function is only limited by the relationship of Eq. (B7). According to [25], this function may be conveniently defined by

$$e(\zeta)=b+2\frac{B-b}{(1+w)N}\left[w\left(\zeta-\frac{1}{2}\right)+(1-w)\left\{\frac{\left(\zeta-\frac{1}{2}\right)^3}{N^2}-\frac{\left(\zeta-\frac{1}{2}\right)^4}{2N^3}\right\}\right], \tag{B10}$$

where the relation of $|d^2e(1/2)/d\zeta^2| \approx |d^2e(N+1/2)/d\zeta^2| \approx 0$ should be satisfied, and w is defined by

$$w=\frac{\left|\frac{de(1/2)}{d\zeta}\right|}{\left|\frac{de(N+1/2)}{d\zeta}\right|}. \tag{B11}$$

b. Finite-difference scheme definition

Substituting $E=e(\zeta)$ into Eq. (B3), we obtain

$$\frac{\partial}{\partial t}n(t,\zeta)e^2(\zeta)\frac{de(\zeta)}{d\zeta}d\zeta=-D(\zeta)\frac{\partial j(t,\zeta)}{\partial\zeta}d\zeta. \tag{B12}$$

The finite-difference scheme should satisfy the mass balance conditions. The energy interval from 0 to E_0 will be divided into N layers, such as the layer frontiers correspond to the half-integer ζ values, so that $e(1/2)=b$, $e(N+1/2)=B$, thus we obtain for each layer

$$\int_{\zeta-1/2}^{\zeta+1/2} n(t,\eta)e^2(\eta)\frac{de(\eta)}{d\eta}d\eta = -D(\zeta)[j(\zeta-1/2)-j(\zeta+1/2)]. \tag{B13}$$

Using a linear interpolation of $de(\zeta)/d\zeta$ on the layer frontiers, and a single-point quadrature to integrate over the layer, we obtain the finite-difference scheme in the form

$$\frac{\partial}{\partial t}n_k=R_{k.k-1}n_{k-1}+R_{k.k}n_k+R_{k.k+1}n_{k+1}, \tag{B14}$$

where

$$n_k=n_k[t,e(k)], \tag{B15}$$

$$R_{k.k-1}=\frac{Q_1(k-1/2)-\frac{Q_2(k-1/2)}{2}}{Q_0(k)}, \tag{B16}$$

$$R_{k.k}=\frac{Q_1(k+1/2)\frac{Q_2(k-1/2)}{2}-\left[Q_1(k+1/2)-\frac{Q_1(k-1/2)}{2}\right]}{Q_0(k)}, \tag{B17}$$

$$R_{k.k+1}=\frac{Q_1(k+1/2)+\frac{Q_2(k+1/2)}{2}}{Q_0(k)}, \tag{B18}$$

$$Q_0(\zeta)=e^2(\zeta)\frac{de(\zeta)}{d\zeta}, \tag{B19}$$

$$Q_1(\zeta)=\frac{D(\zeta)e^2(\zeta)}{\frac{de(\zeta)}{d\zeta}}, \tag{B20}$$

$$Q_2(\zeta)=Q_1(\zeta)\frac{\partial\psi}{\partial\zeta}.$$

It follows from the above equations that

$$j(t,\zeta)=Q_1(\zeta)n(t,\zeta). \tag{B21}$$

In order to incorporate the boundary conditions represented by Eqs. (23), the finite-differences scheme should be defined from $k=1$ to $k=N$.

c. Properties of the finite-difference scheme

Let us define the matrix $\hat{R}$ and the vector $\vec{n}$ with their respective components R_{mn} and n_k. Using these notations, the finite-difference scheme may be rewritten as

$$\frac{\partial}{\partial t}\vec{n}(t)=\hat{R}(t)\vec{n}(t). \tag{B22}$$

Let us analyze this equation when $\hat{R}$ is independent of t. The solution of Eq. (B22) yields

$$\vec{n}(t)=\exp[\hat{R}t]\vec{n}(0). \tag{B23}$$

If $\hat{R}$ can be represented by

$$\hat{R}=\hat{U}\hat{\lambda}\hat{V}' \tag{B24}$$

then the solution will be

$$\vec{n}(t)=\hat{U}\exp[\hat{\lambda}t]\hat{V}'\vec{n}(0), \tag{B25}$$

where $\hat{\lambda}$ is the diagonal matrix of the eigenvalues, and $\hat{U}$ is the matrix of the right eigenvectors,

$$\hat{R}\hat{U}=\hat{U}\hat{\lambda} \tag{B26}$$

and $\hat{V}'$ the matrix of the left eigenvectors,

$$\hat{V}'\hat{R}=\hat{\lambda}\hat{V}'. \tag{B27}$$

It follows from Eq. (B25) that $\vec{n}(t)$ is a linear combination of exponential functions.

2. The matrix exponent method

If the coefficient of the initial differential equation is constant, then the $\hat{R}$ operator is also time independent. In this case, the solution is given by Eq. (B25). In fact, such a solution might be sufficient for our purposes. In practice, the need to calculate the eigenvectors may preclude direct usage of Eq. (B25). Before attempting the matrix diagonalization, we shall have to symmetrize the $\hat{R}$ matrix. If we find a diagonal operator $\hat{F}$ to perform the required transformation, the resulting matrix

$$\hat{\upsilon}=\hat{F}^{-1}\hat{R}\hat{F} \tag{B28}$$

will be symmetric. In this case, the eigenvalues of $\hat{\upsilon}$ are the same as those of $\hat{R}$, as the diagonal transformation discussed does not change the secular equation. Thus,

$$\hat{\upsilon}\hat{T}=\hat{T}\hat{\lambda}, \tag{B29}$$

where $\hat{T}$ is the matrix of the eigenvectors of $\hat{\upsilon}$. Since the $\hat{\upsilon}$ matrix is symmetric, the right and the left vectors are the same, so

$$\hat{\lambda}=\hat{T}^{-1}\hat{\upsilon}\hat{T}=\hat{T}^{-1}\hat{F}^{-1}\hat{R}\hat{F}\hat{T}. \tag{B30}$$

On the other hand,

$$\hat{\lambda}=\hat{V}'\hat{R}\hat{U} \tag{B31}$$

or

$$\hat{V}'=\hat{T}'\hat{F}^{-1}, \tag{B32}$$

$$\hat{U}=\hat{F}\hat{T}, \tag{B33}$$

$$\exp[\hat{R}t]=\hat{F}\hat{T}\exp[\hat{\lambda}t]\hat{T}'\hat{F}^{-1}. \tag{B34}$$

To determine the operator $\hat{F}$, we have to go back to Eq. (B28). Taking into account that $F_{ij}=F_i\delta_{ij}$, for $j=i+1$, we obtain

$$\upsilon_{ij}=R_{ij}\left(\frac{F_j}{F_i}\right), \quad \upsilon_{ji}=R_{ji}\left(\frac{F_i}{F_j}\right). \tag{B35}$$

Since we have $\upsilon_{ij}=\upsilon_{ji}$, then we obtain from the above equations:

$$F_{i+1}=F_i\sqrt{\frac{R_{j+1,i}}{R_{i,i+1}}}, \quad F_1=1, \tag{B36}$$

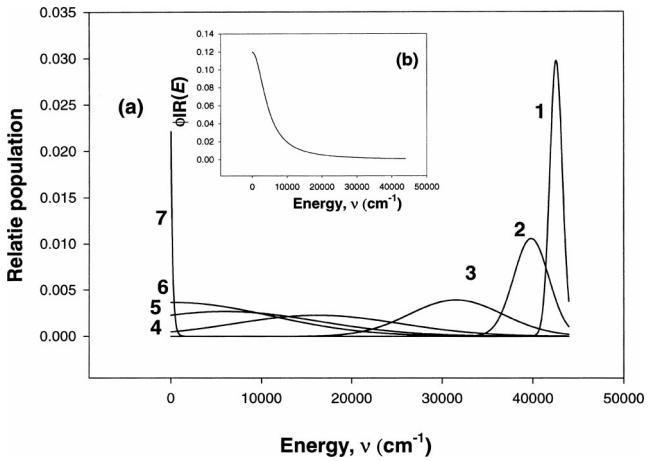

FIG. 11. (a) Time evolution of the population distribution, $P=20$ mTorr, other model parameters are given in the text. Distributions 1 to 7 were modeled for the times of 10, 30, 60, 100, 600, 1400, and 2500 μs after the excitation. (b) The inset shows the energy dependence of the IR emission yield, calculated using the experimental IR emission kinetics and the modeled time dependence of the population distribution.

$$\upsilon_{ij}=\upsilon_{ji}=\sqrt{R_{ij}R_{ji}}, \tag{B37}$$

$$\upsilon_{ii}=R_{ii}. \tag{B38}$$

Thus, using the approach presented and the dynamic parameters already estimated above, we can calculate the $n(t,E)$ distribution function at any instant of time.

3. Calculations

Figure 11 shows the time evolution of the distribution function, calculated using the estimated values of the dynamic parameters. Note that the distribution maximum moves towards lower energies with simultaneous growth of the distribution width, although the solution eventually collapses into the Boltzmann distribution. Using the data of Fig. 11, we calculated the energy dependence of the IR emission yield,

$$\phi_{IR}(E)=\frac{1}{1+\upsilon(E)}. \tag{B39}$$

This latter function is also plotted in Fig. 11. Here $\upsilon(E)$ is the ratio of the collision-induced relaxation rate over the vibronic spectrum, to the IR emission rate. It is very important to note that the approach proposed permitted to determine the $\upsilon(E)$ function. The function obtained, though, is but a semiquantitative approximation, as the dynamic parameters used in its calculation have been estimated only quite roughly. We should additionally note that the experimental $\phi_{IR}(E)$ function is dependent on the IR detector sensitivity, which is unaccounted for: we stated that the detector is sensitive in the 833–1250 cm^{-1} range, its sensitivity being dependent on the IR photon energy.

[1] L.D. Landau and E.M. Lifshits, *Quantum Mechanics. III. Nonrelativistic Theory* (Mir, Moscow, 1989).
[2] C.H. Townes and E.A.L. Schawlow, *Microwave Spectroscopy* (Dover, New York, 1995).
[3] M. Goldman, *Quantum Description of High Resolution NMR in Liquids* (Oxford Science Publications, Oxford, 1990).
[4] N. Ohta and T. Takemura, J. Phys. Chem. **94**, 3466 (1990).
[5] H. Abe and H. Hayashi, J. Phys. Chem. **98**, 2797 (1994).
[6] T. Imamura, N. Tamai, Y. Fukuda, I. Yamazaki, S. Nagakura, H. Abe, and H. Hayashi, Chem. Phys. Lett. **135**, 208 (1987).
[7] V.I. Makarov, Chem. Phys. **271**, 79 (2001).
[8] A. Matsuzaki and S. Nagakura, Helv. Chim. Acta **61**, 675 (1978).
[9] H. Abe and H. Hayashi, Chem. Phys. Lett. **206**, 337 (1993).
[10] V.I. Makarov, A. Cruz, and E. Quinones, Chem. Phys. **264**, 101 (2001).
[11] V.P. Krainov and B.M. Smirnov, *Radiation Processes in Atomic Physics* (Highest School, Moscow, 1983).
[12] P.G. Green, Ph.D. thesis, Massachusetts Institute of Technology, 1989 (unpublished).
[13] J.K.G. Watson, M. Herman, J.C. Van Creen, and R. Colin, J. Mol. Spectrosc. **95**, 101 (1982).
[14] M. Fuji, A. Haijima, and M. Ito, Chem. Phys. Lett. **150**, 380 (1988).
[15] V.I. Makarov, S.A. Kochubei, V.N. Ishchenko, and I.V. Khmelinskii, J. Chem. Phys. **113**, 128 (2000).
[16] L. Allen and H. Eberly, *Optical Resonance and Two Level Atoms* (Wiley, New York, 1975).
[17] T. Suzuki and N. Hashimoto, J. Chem. Phys. **110**, 2042 (1999).
[18] J. Segal, Y. Wen, R. Lavi, R. Singer, and C. Wittig, J. Phys. Chem. **95**, 8078 (1991)
[19] D.L. Holterman, E.K.C. Lee, and K. Nanes, J. Chem. Phys. **77**, 5328 (1982).
[20] D. Qin, G.V. Hartland, and H.L. Dai, J. Phys. Chem. **104**, 10 460 (2000).
[21] D. Qin, G.V. Hartland, C.L. Chen, H.L. Dai, Z. Phys. Chem. **214**, 1501 (2000).
[22] B. Xue, J. Han, and H.L. Dai, Phys. Rev. Lett. **84**, 2606 (2000).
[23] J.B. Peterson and J.H. Freed, J. Chem. Phys. **61**, 1517 (1974).
[24] Z. Shulton and K. Shulton, J. Chem. Phys. **66**, 4616 (1977).
[25] S.B. Krisinel and N.B. Shohirev, Solution of the Nonstationary Diffusion Equation by the Finite Differences Method, Novosibirsk, Russia, 1987.